Laning Transitions in Pattern Forming Driven Binary Systems with Competing Interactions

C. Reichhardt and C. J. O. Reichhardt

Theoretical Division and Center for Nonlinear Studies,

Los Alamos National Laboratory, Los Alamos, New Mexico 87545, USA

(Dated: October 21, 2025)

A binary system of particles that move in opposite directions under an applied field can exhibit disordered states as well as laned states where the particles organize into oppositely moving high-mobility lanes to reduce collisions. Previous studies of laning transitions generally focused on particles with purely repulsive interactions. Here, we examine laning transitions for oppositely moving pattern-forming systems of particles with competing attractive and repulsive interactions, which in equilibrium form crystal, stripe, and bubble states. In addition to multiple types of laned states, we find jammed crystals, stripes, and bubbles, and generally observe a much richer variety of phases compared to the purely repulsive system. In the stripe forming regime, the system can dynamically reorder into oppositely moving stripes that are aligned in the direction of the drive. The bubble phase can produce strongly polarized jammed states of elongated bubbles where particles in the individual bubbles segregate to opposite sides of the bubbles. We also find disordered states, segregated laned bubble states where the bubbles pass each other in lanes, and segregated bubbles that move through one another. In the compact bubble regime, we obtain a plastic bubble state in which the oppositely driven particles remain trapped in the bubbles but the bubbles move past each other at a slow velocity due to a net imbalance in the bubble population. At higher drives, individual particles begin to jump from bubble to bubble. We show that the different phases and the transitions between them produce signatures in the velocity-force and differential mobility curves. We demonstrate that the critical force for escaping from the jammed state is nonmonotonic, with stripes exhibiting the lowest unjamming force.

I. INTRODUCTION

In a binary assembly of repulsively interacting particles, such as Yukawa particles, subjected to a drive that causes the particles to move in opposite directions, a variety of nonequilibrium phases can appear. At lower drives, these phases are fluid-like, but for higher drives there can be a dynamically phase-separated laned state in which the particles segregate into extended lanes that move past each other [1–9]. This type of laning has been studied for colloidal particles [10-14], dusty plasmas [15], multicomponent magnetic skyrmion systems [16], and driven hard disks [17]. Laning dynamics can also appear in models of pedestrian flows [18, 19] and binary driven active matter systems [20–22]. Under certain conditions, dense clusters can span the system at lower drives, leading to the formation of a jammed state [17] or the appearance of intermittent jamming in which isolated groups of particles cannot get past one another [9, 14, 23]. Oppositely driven binary hard disk systems can also exhibit jammed, disordered, and fully phase-separated laned states, and the transitions between these states produce jumps in the velocity-force curves [17]. Binary active disk systems in which the two species are driven in opposite directions also produce disordered laned states as well as motility-induced phase-separated states that coexist with laning [17]. Laning transitions can also be induced with ac driving [24, 25]. When an additional chirality is introduced, such that particles move preferentially to one side when interacting with other particles, there can be transitions to tilted lane states. Effects of this type have been observed for flows of pedestrians with chiral interaction rules [19] and in binary driven skyrmion systems where the chirality arises from a Magnus force [16, 26].

Most laning studies have been performed for particles with purely repulsive interactions, such as screened Coulomb interactions or hard disks, but there have also been studies in binary systems with longer-range attraction, such as Lennard-Jones interactions, where jammed, laned, disordered, and partially laned states can arise as a function of drive and particle density [27]. Laning has also been studied in binary driven dipolar systems, where a correlation appears between the chaining from the dipolar interactions and dynamically induced laning [28]. An open question is what are the dynamic phases and laning states for a binary assembly of particles with more complex interactions that are driven in opposite directions. These interactions could include competing short-range attraction and long-range repulsion (SALR), which leads to the formation of a variety of different mesophases in the absence of driving, such as anisotropic crystals, bubbles, stripes, and void lattices [29-40]. Similar mesophase pattern can arise even for purely repulsive interaction potentials as long as the interaction potential is composed of two steps or has two distinct length scales [41–43]. SALR interactions can appear in soft matter and biological systems [40, 44, 45]. In addition, a variety of hard condensed matter systems can be described in terms of particles with competing interactions or with multiple length scale interactions. For example, bubble and stripe states are predicted to form in electron liquid crystals [46-51] and multi-component superconducting vortex systems [52–56].

In this work, we consider laning transitions in an oppositely driven binary assembly of particles with SALR interactions composed of both long-range and very shortrange Coulomb repulsion and an intermediate-range attraction. For a fixed ratio of attraction to repulsion, and in the absence of driving, the system forms bubbles, stripes, a void lattice, and finally a dense uniform crystal as a function of increasing particle density. For increasing attraction and fixed density, we find a uniform crystal, a stripe phase, and finally a bubble phase, where the bubbles decrease in size as the attractive term becomes larger [32, 35–37, 57]. This same model has also been studied with the addition of a periodic quasi-one-dimensional substrate [58] or ratchet potential [59], which introduces additional length scales. In previous work, single species SALR particle assemblies subjected to uniform dc driving over random or periodic substrates exhibited pinned, disordered flow, and dynamically ordered states [31, 58]. In this work, we focus on the dynamical evolution of the patterns when half of the particles are driven in a direction opposite to that of the other half, and compare it to the laning transitions found in purely repulsive systems. A much richer variety of states arises in the SALR system. At zero attraction, we find phases similar to those produced by repulsive Yukawa particles. For finite competing interactions, a number of dynamical states appear in the stripe and bubble regimes, including disordered flow, fully segregated lanes, and mixed laning states. We find that driving can disorder a jammed stripe phase and cause a dynamical reorientation into stripes aligned with the drive, but with laning occurring within each stripe. For bubbles, even in the jammed phase we observe a rearrangement of the particles in the bubbles, which segregate to form a polarized bubble state. In the bubble regime we also find a disordered fluid state, a segregated bubble state with lanes of bubbles, and segregated states in which the bubbles move through each other. The different phases and the transitions between them produce signatures in the velocity versus drive and differential mobility versus drive curves, as well as changes in the density of topological defects and the flow patterns.

II. SIMULATION

We model a two-dimensional system of size $L \times L$ with periodic boundary conditions in the x and y directions and with L=36. The system contains N particles that have a SALR interaction potential with a long-range repulsive Coulomb term and a short-range attractive term, given by:

$$V(R_{ij}) = \frac{1}{R_{ij}} - B \exp(-\kappa R_{ij}) . \tag{1}$$

Here, $R_{ij} = |\mathbf{R}_i - \mathbf{R}_j|$ is the distance between particles i and j. The first term is the long-range repulsion, which favors the formation of a triangular lattice, and the second term is the attraction, which can be varied by

changing the strength of the attraction coefficient B and the inverse correlation length κ . Unless otherwise noted, we set $\kappa=1.0$. The particle density is $\rho=N/L^2$. We initialize the system by placing the particles in a triangular lattice and allowing them to relax into crystal, stripe, or bubble phases depending on the values of ρ , B, and κ , as studied in previous work [37, 58].

The particle dynamics evolves via integrating the following overdamped equation:

$$\eta \frac{d\mathbf{R}_i}{dt} = -\sum_{j \neq i}^{N} \nabla V(R_{ij}) + \mathbf{F}_{DC}^i.$$
 (2)

We set the damping coefficient to $\eta=1.0$. The driving force $\mathbf{F}_{\mathrm{DC}}^{i}=\sigma_{i}F_{D}\hat{x}$, where $\sigma_{i}=+1$ for half of the particles and $\sigma_{i}=-1$ for the other half. In most of the simulations reported here, we start with $F_{D}=0$ and gradually increase F_{D} by an increment of $\Delta F_{D}=0.005$ every 10^{4} simulation time steps. When the particle density is low, we consider smaller values of ΔF_{D} and longer time averages. For other simulations, after initializing the system we apply a constant F_{D} . We measure the time-averaged velocity for only the $\sigma=+1$ particles, $\langle V \rangle = (2/N) \sum_{i=1}^{N} \delta(\sigma_{i}-1) (\mathbf{v}_{i} \cdot \hat{\mathbf{x}})$, where \mathbf{v}_{i} is the velocity of particle i. When the ratio of $\sigma_{i}=+1$ and $\sigma_{i}=-1$ particles is 50:50, as we consider here, the corresponding velocity response of the $\sigma=-1$ particles is the same as that of the $\sigma=+1$ particles but reversed in sign. We note that for other ratios, the velocity-force curves can have different slopes for the different particle species.

III. RESULTS

We first consider particles with a purely repulsive Coulomb interaction, obtained by setting B = 0.0. The behavior is expected to be similar to what has been found in previous studies of repulsive laning particles, such as for particles with Yukawa interactions [2–4]. In Fig. 1(a), we plot the velocity-force curve for a system with $\rho = 0.441$. At low drives there is a jammed region with $\langle V \rangle = 0.0$, and the unjamming transition or onset of motion occurs near $F_D = 0.225$, where $\langle V \rangle$ becomes finite. A fluctuating velocity regime of disordered or moving fluid flow occurs for $0.225 < F_D < 0.78$, and there is a high-drive linear region for $F_D > 0.78$ where the velocity fluctuations are strongly reduced and the system enters a laned state. Figure 1(b) shows the corresponding $d\langle V\rangle/dF_D$ versus F_D curve, where we have performed a running average over five driving force increments to smooth the curve. This measure exhibits a clear peak near the jammed-unjammed transition, has strong fluctuations in the moving fluid regime, and shows a final cusp near the transition to the laned state. In Fig. 1(c) we plot the fraction of sixfold coordinated particles $P_6 = N^{-1} \sum_{i=1}^{N} \delta(z_i - 6)$ versus F_D , where the particle coordination number z_i is obtained from a Voronoi construction of the particle positions. In the jammed

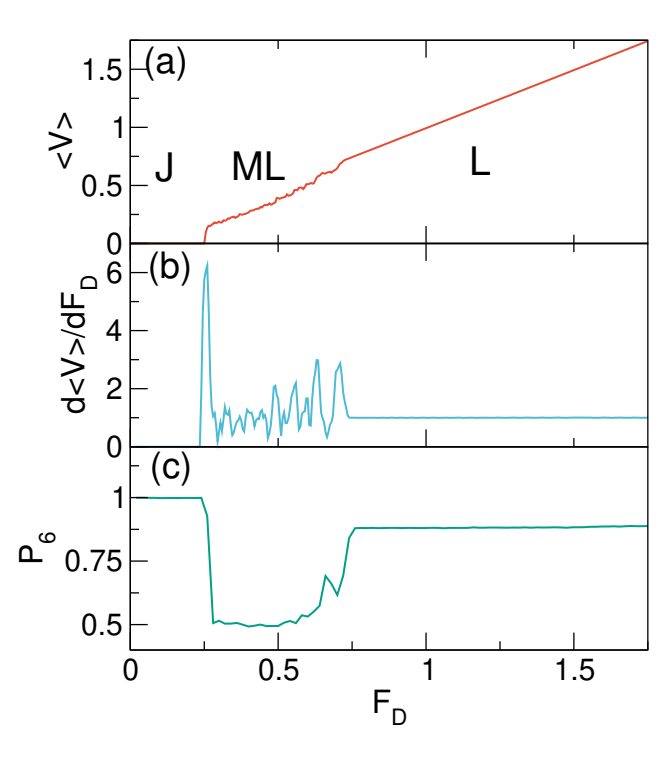


FIG. 1. (a) Velocity $\langle V \rangle$ vs drive F_D for oppositely driven SALR particles at a density of $\rho=0.441$ with B=0.0 in the purely repulsive Coulomb interaction regime. Region J is the jammed phase shown in Fig. 2(a), ML is the moving liquid phase shown in Fig. 2(b), and L is the laned phase shown in Fig. 2(c). (b) The $d\langle V \rangle/dF_D$ vs F_D curve more clearly shows the transitions among phases J, ML, and L. (c) The fraction of sixfold-coordinated particles, P_6 , vs F_D also shows signatures of the three phases.

phase, P_6 is close to 1.0, consistent with the system forming a jammed triangular lattice, as shown in Fig. 2(a) at $F_D = 0.05$. At the unjamming transition, P_6 drops when the system breaks up into a partially segregated fluid-like state, shown in Fig. 2(b) at $F_D = 0.4$. In this moving liquid phase, the triangular ordering is lost, and there are numerous topological defects along with large velocity fluctuations. Additionally, the frequent collisions between particles that occur in this fluctuating phase cause $\langle V \rangle / \eta F_D$ to be much less than one. For a completely free particle interacting with no other particles, we would have $\langle V \rangle / \eta F_D = 1.0$. The onset of the laned state correlates with a jump up in P_6 and is also where $d\langle V \rangle/dF_D$ approaches 1.0, which indicates reduced drag. Figure 2(c) shows the particle configurations in the laned state at $F_D = 1.5$, where large blocks of particles are all moving in the same direction along well-defined lanes. There is triangular ordering of the particles within the lanes, which leads to the increase in P_6 to $P_6 = 0.9$ at the onset of the laned state in Fig. 1(c). There is not complete ordering of the particles, since the boundaries separating lanes moving in opposite directions contain aligned dislocations that glide as the crystallites slip past one another.

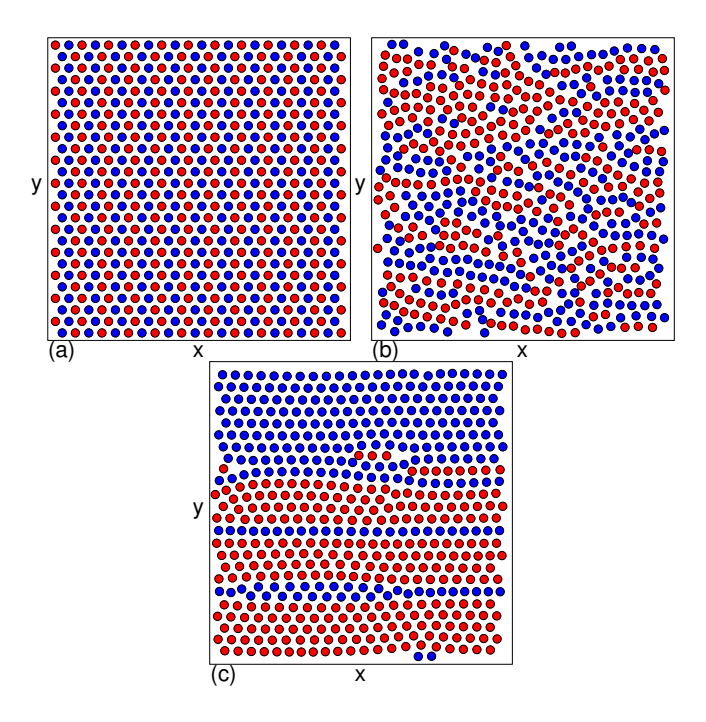


FIG. 2. Particle positions for the system from Fig. 1 at $\rho = 0.441$ and B = 0.0, where the particles have only a Coulomb repulsion. Red (blue) particles are driven in the negative (positive) x direction. (a) The jammed phase J at $F_D = 0.05$. (b) The moving liquid ML at $F_D = 0.4$. (c) The segregated laned state L at $F_D = 1.5$. Note that the radius of the circles representing the particles has been chosen for visual clarity here and throughout this work.

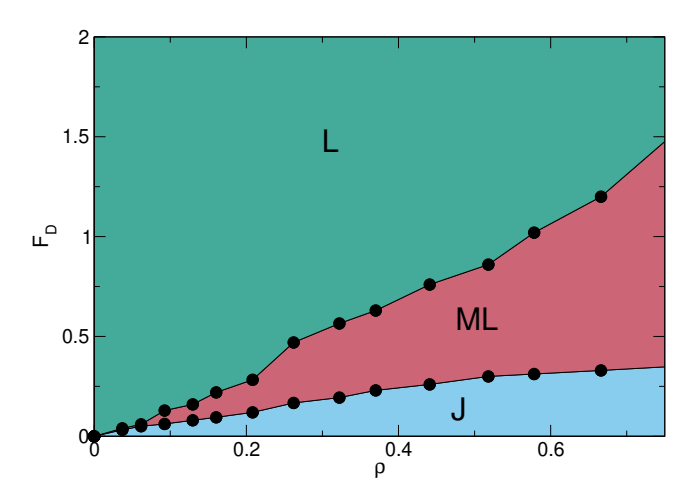


FIG. 3. Dynamic phase diagram as a function of F_D vs ρ for the system from Fig. 1 with B=0.0. J: jammed state (blue); ML: moving liquid (red); and L: the higher drive laned state (green).

We performed a series of simulations for the system in Fig. 1 at varied particle density ρ , and from the features in the transport curves and P_6 , we map out the evolution of the three phases, shown in Fig. 3 as a function of F_D versus ρ . The critical unjamming force F_c sep-

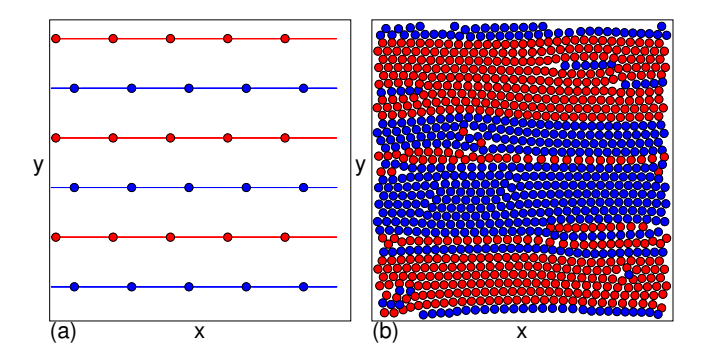


FIG. 4. Particle positions for the system from Fig. 3. Red (blue) particles are driven in the negative (positive) x direction. (a) At $\rho=0.037$ and $F_D=0.5$, the system has fully segregated into one-dimensional (1D) lanes. Here the particle trajectories are also plotted as colored lines indicating the direction of drive, with red for $\sigma_i=-1$ and blue for $\sigma_i=+1$. (b) The laned state at $\rho=0.86$ and $F_D=1.6$.

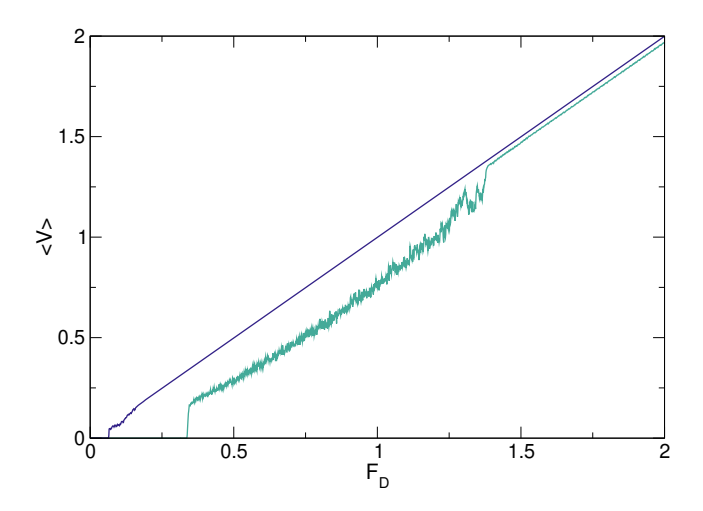


FIG. 5. $\langle V \rangle$ vs F_D for the system from Fig. 4 with B=0.0 at $\rho=0.037$ (blue) and $\rho=0.86$ (green). For the higher density $\rho=0.86$, there is an extended regime of the moving liquid state and a sharper transition into the laned state at higher drives.

arating the jammed and moving liquid phases increases with increasing ρ , and the drive at which the onset of the laning phase occurs also increases. At lower ρ , we find some states where the system can form single-file one-dimensional (1D) lanes, as shown in Fig. 4(a) at $\rho = 0.037$ and $F_D = 0.5$. When the density is higher, the lanes are wider, as illustrated in Fig. 4(b) for $\rho = 1.0$ at $F_D = 1.6$. The emergence of thinner lanes for lower ρ may reflect the fact that the smaller number of particles present can dynamically anneal into a well-ordered state very effectively, and/or that thicker lanes are destabilized by the Coulomb repulsion. In Fig. 5, we plot $\langle V \rangle$ versus F_D for the system from Fig. 4 at $\rho = 0.037$ and $\rho = 0.86$. For the higher density, there is an extended range of disordered flow and a sharper transition into the laned state, as indicated by the jump up in $\langle V \rangle$.

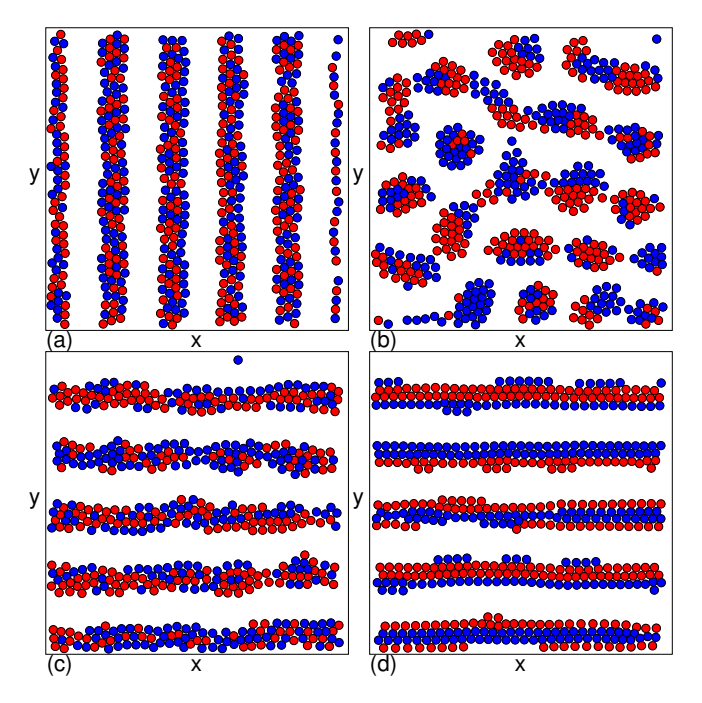


FIG. 6. Particle positions for the stripe regime at B=2.1 and $\rho=0.441$ in different dynamical phases. Red (blue) particles are driven in the negative (positive) x direction. (a) The stripe state at $F_D=0.0$. (b) A disordered state at $F_D=0.072$. (c) The disordered stripe phase at $F_D=0.6$. (d) A laned stripe state at $F_D=1.0$.

Wide lanes were also observed in systems of oppositely moving disks [17]; however, one difference is that the jammed phases for the disks are highly heterogeneous and are composed of coexisting high- and low-density regions. In contrast, for the Coulomb system, the jammed state is homogeneous. This is because the long-range Coulomb repulsion penalizes significant density fluctuations in the system. The disk system also had a critical density below which jamming does not occur [17], while for the Coulomb system, a jammed phase is present down to arbitrarily low densities. This is also a consequence of the long-range Coulomb interactions. Even at zero drive in two dimensions (2D), there is a finite density for solidification or jamming transitions to occur in hard disk systems [60]. In work on gliding dislocations moving in opposite directions, it was found that due to the long-range strain field, the dislocations could jam at arbitrarily low densities [61], which is consistent with the idea that it is always possible to reach a jammed state in a Coulomb system. We also note that features in the velocity-force curves, peaks in $d\langle V \rangle/dF_D$, and changes in P_6 have been used previously to identify different dynamic phases and transitions between these phases in driven particle systems with quenched disorder [62].

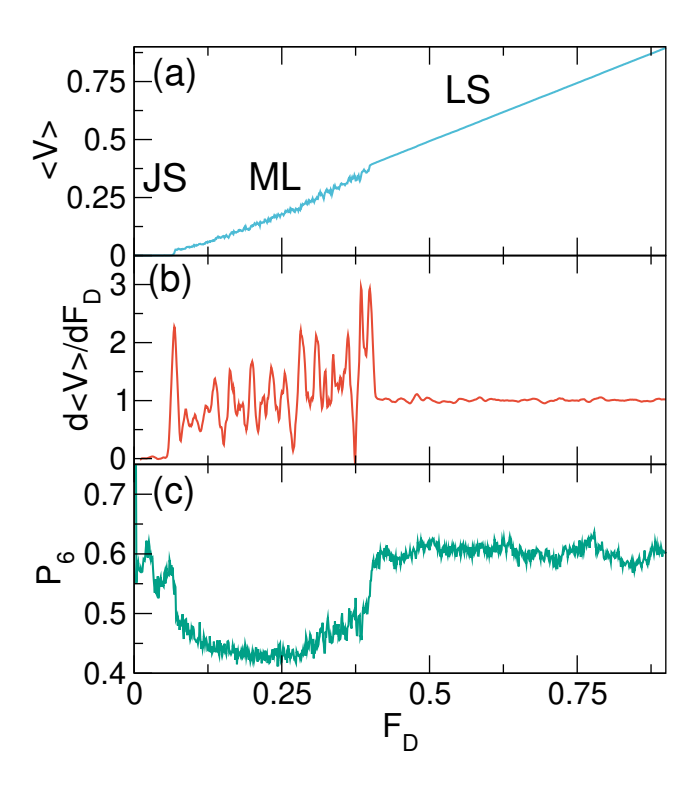


FIG. 7. $\langle V \rangle$ vs F_D curves for the stripe-forming system from Fig. 6 with B=2.1 and $\rho=0.441$. (b) The corresponding $d\langle V \rangle/dF_D$ vs F_D . (c) The corresponding P_6 vs P_D .

IV. STRIPE STATE

We next consider particles that have both repulsive and attractive interactions. For B < 1.9, the dynamic phases we observe are similar to those described in Sec. III for the B = 0.0 system, with a jammed uniform state, a moving liquid state, and a higher-drive laned state. For 1.9 < B < 2.25, the system forms a jammed stripe state, as shown in Fig. 6(a) at $F_D = 0.0$ for B = 2.1and $\rho = 0.441$. As F_D is increased, the jammed phase breaks up into a disordered phase, illustrated in Fig. 6(b) at $F_D = 0.072$. At higher drives, stripes reform, but these stripes are are now oriented in the direction of the drive, as shown in Fig. 6(c) at $F_D = 0.6$. The oriented stripes fluctuate rapidly and contain a varying number of particles that are exchanging places, so that the system is in a fluctuating quasi-one-dimensional fluid rather than a laned state. At the highest drives, the stripes settle into well-ordered stable lanes where the particles within each stripe travel in opposite directions to each other along segregated lanes, as imaged in Fig. 6(d) at $F_D = 1.0$. The transport curve signatures produced by the different phases are shown in Fig. 7(a), where we plot $\langle V \rangle$ versus F_D . The transitions are more clearly highlighted in the corresponding plot of $d\langle V \rangle/dF_D$ versus F_D in Fig. 7(b), where multiple peaks appear. In the laned stripe phase, $d\langle V\rangle/dF_D$ is close to one, indicating almost linear flow. The amount of topological order varies somewhat in the

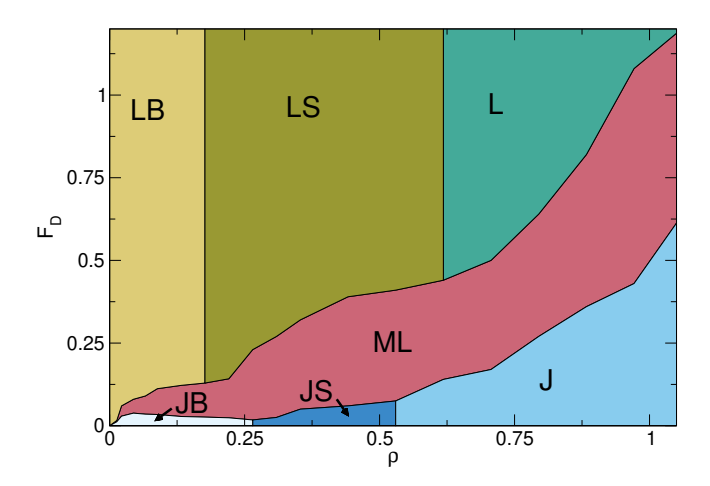


FIG. 8. Dynamic phase diagram as a function of F_D vs ρ for a system with B=2.0. JB: jammed bubble phase (pale blue), JS: jammed stripe phase (dark blue), J: jammed uniform phase (medium blue), ML: disordered moving liquid phase (red), LB: laned bubble phase (yellow), LS: laned stripe phase (olive green), and L: laned state (green).

different dynamic stripe states, which are visible in the P_6 versus F_D curve shown in Fig. 7(c). The order is lowest in the disordered flow state, but even in the laned stripe phase, the value of P_6 is lower than in the corresponding laned phase for the B = 0.0 system in Fig. 1(c). The laned stripe phase appears when 1.9 < B < 2.35, and also occurs for values of B at which the jammed state is a bubble state rather than a stripe state. This occurs because the application of driving can stretch the bubbles into stripes. From the transport curves and P_6 , it is not possible to distinguish the 2D disordered fluctuating state just above unjamming from the disordered stripe state, so we lump the 2D moving liquid and quasione-dimensional moving liquid together into a disordered moving liquid phase. We note that it may be possible to use machine learning techniques to delineate a transition between these two liquid states [63].

In Fig. 8, we map out the dynamic phase diagram as a function of F_D versus ρ for a system with B=2.0. At finite B, the system undergoes transitions between different ground states as a function of ρ when $F_D = 0.0$. When B = 2.0, the system shows a jammed bubble state for $\rho < 0.25$, a stripe phase for $0.25 \le \rho \le 0.53$, and a uniform jammed phase for $\rho > 0.53$. The unjamming transition is nonmonotonic as a function of ρ in Fig. 8, initially rising in the bubble state, passing through a local minimum near the jammed bubble to jammed stripe transition, and then increasing more rapidly in the uniform jammed state. The jammed bubble phase unjams into a disordered state, and at higher drives, a laned bubble state arises, as illustrated in Fig. 9(a) at $\rho = 0.0926$ and $F_D = 0.25$. For the same drive of $F_D = 0.25$ at $\rho = 0.16$, Fig. 9(b) shows that there is some partial stripe ordering. An ordered stripe state appears at $F_D = 0.25$ and $\rho = 0.26$ in Fig. 9(c), while Fig. 9(d) shows a high

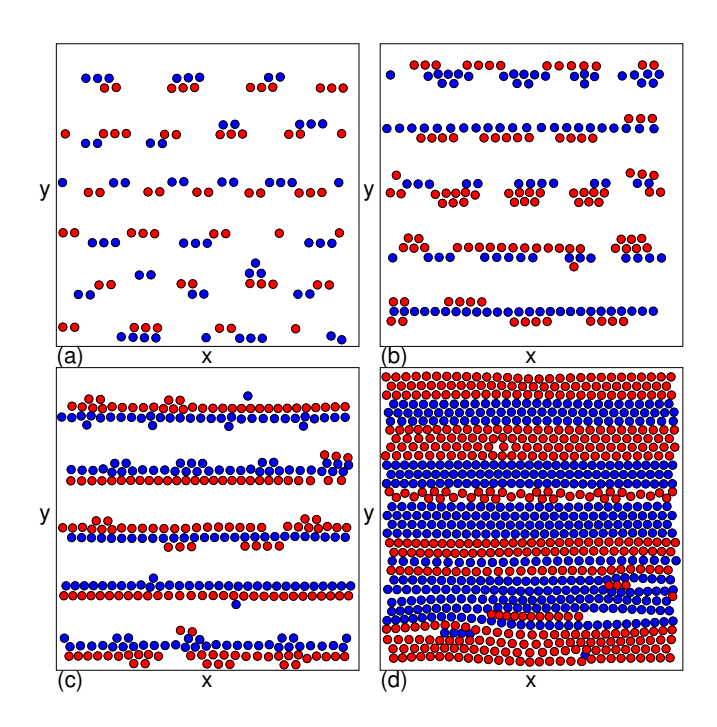


FIG. 9. Particle positions for the B=2.0 system from Fig. 8. Red (blue) particles are driven in the negative (positive) x direction. (a) The laned bubble state at $\rho=0.0926$ and $F_D=0.25$. (b) The laned bubble state at $\rho=0.16$ and $F_D=0.25$, where partial stripe ordering appears. (c) The laned stripe state at $\rho=0.26$ and $F_D=0.5$. (d) The uniform laned state at $\rho=0.76$ and $F_D=1.0$.

drive uniform laned state at $\rho = 0.76$ and $F_D = 1.0$. For $0.17 \le \rho \le 0.65$, the high-drive state is a laned stripe state instead of a laned uniform state. Due to the fact that the drive elongates the bubbles into stripes, the extent of the laned stripe state exceeds that of the $F_D = 0$ stripe state, which spans only the range $0.25 \le \rho \le 0.53$.

V. VARIED INTERACTIONS

We next consider systems with fixed $\rho = 0.44$ and varied B ranging from the purely repulsive B = 0.0 case to large B values for which a bubble state is present. In the absence of a drive, the system forms a uniform crystal for $0 < B \le 1.9$, stripes for $1.9 \le B < 2.3$, and bubbles for $B \geq 2.3$. In Fig. 10, we plot the critical unjamming force F_c versus ρ , with vertical lines highlighting the locations of the $F_D=0$ crystal, stripe, and bubble phases. The unjamming force F_c is a strongly nonmonotonic function of B and is affected by the type of pattern that forms in the system. There is a gradual decrease of F_c with increasing B throughout the uniform crystal phase, followed by a more rapid drop to a local minimum in F_c on the low-B end of the stripe state near B=2.0. As B continues to increase, F_c grows throughout the stripe phase and then begins to increases more rapidly once the system transitions into the bubble phase. A local dip in F_c appears

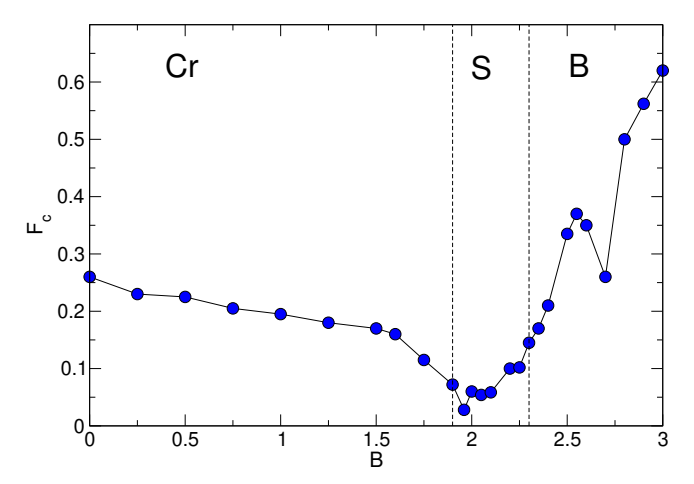


FIG. 10. The critical unjamming force F_c vs B for a system with $\rho = 0.441$. The vertical dashed lines indicate where the system forms jammed crystal (Cr), stripe (S), and bubble (B) states. F_c varies non-monotonically with B.

in the bubble phase near B=2.7 corresponding to the onset of plastic bubble depinning, where particles remain trapped in individual bubbles but the bubbles themselves move past each other. In previous work, a similar nonmonotonic depinning threshold was observed for SALR particles interacting with a periodic one-dimensional substrate, where the depinning force reaches a maximum in the stripe phase and then falls off rapidly in the bubble phase [58]. This is consistent with what we find in Fig. 10, where the stripe phase is the softest phase and has the lowest elastic constant, which causes the unjamming force to be low but would also produce a local maximum in the depinning force when a substrate is present. The phase we observe here is a jammed rather than a pinned state, since the system contains no quenched disorder. The jamming arises purely from the interaction of the particles that are attempting to move in opposite directions. It is possible that for values of B larger than those considered here, F_c would drop again when the radii of the bubbles begins to shrink due to the very strong attractive term.

Based on the transport curves, P_6 , and images of the particles, we construct a dynamic phase diagram as a function of F_D versus B for the $\rho = 0.441$ system in Fig. 11. For B < 1.9, there is a uniform jammed phase, a disordered moving liquid phase, and a uniform laned phase, similar to what is found for the B = 0.0 system in Fig. 2. For 1.9 < B < 2.3, there is a jammed stripe phase, a disordered moving liquid phase, and an ordered laned stripe state. The laned stripe phase persists up to B = 2.3, even though a jammed bubble state forms for B > 2.2. This occurs because the bubbles become elongated in the driven state and merge to form a stripe. The drive at which the ordered laned stripe phase arises passes through a peak at B = 2.35, which also corresponds to the value of B that separates the lower Blaned stripe state from the higher B laned bubble state.

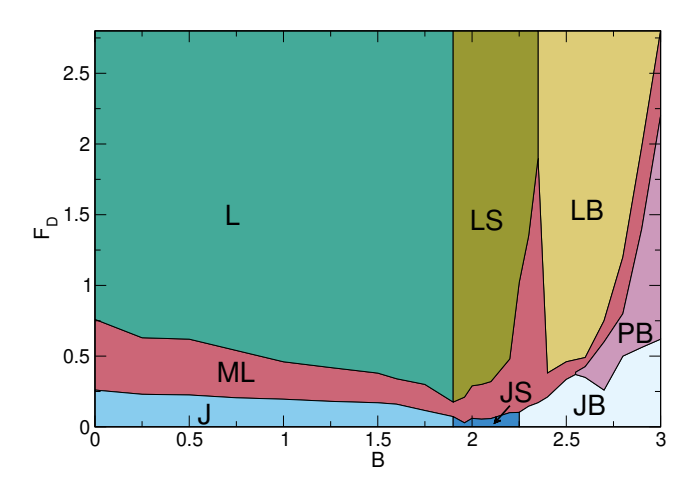


FIG. 11. Dynamic phase diagram as a function of F_D vs B for a system with $\rho=0.441$. JB: jammed bubble phase (pale blue), JS: jammed stripe phase (dark blue), J: jammed uniform phase (medium blue), ML: disordered moving liquid phase (red), LB: laned bubble phase (yellow), LS: laned stripe phase (olive green), L: laned state (green), and PB: plastic bubble phase (purple).

At B = 2.35, the jammed bubble state contains bubbles in which the two particle species are evenly spatially distributed, as shown in Fig. 12(a) for $F_D = 0.03$. As the drive increases, the particles gradually rearrange to form a polarized jammed bubble state, with the $\sigma = -1$ particles accumulating on the left side of each bubble and the $\sigma = +1$ particles accumulating on the right side of each bubble, as shown in Fig. 12(b) at $F_D = 0.1$. The attractive interaction term prevents the bubbles from tearing apart. At higher drives, the system forms a disordered bubble flow phase in which the bubbles move past each other, and eventually a high-drive bubble phase containing a small number of stripes emerges, as illustrated in Fig. 12(c) at $F_D = 2.5$. Here the bubbles have become fully segregated by species. Figure 12(d) shows a laned segregated stripe state at B = 2.25 and $F_D = 1.5$. The drive at which full species segregation occurs increases near the boundary between the laned stripe and laned bubble states. In Fig. 13, we plot $\langle V \rangle$ and $d\langle V \rangle/dF_D$ versus F_D for the same system at B = 2.35, showing the jammed bubble, fluctuating moving liquid, and laned bubble states. For clarity, we have performed a running average over the nearest five points on the differential mobility curve.

For 2.25 < B < 2.6, the jammed bubble state unjams into a disordered moving liquid phase, while for $B \geq 2.6$, the unjamming occurs via the formation of a plastic bubble phase, where particles remain trapped in individual bubbles but the bubbles move past each other. The segregation of the particles into distinct bubbles can occur in two ways. In the first, the bubbles tear apart along the direction perpendicular to the drive, as shown in Fig. 14(a) for B = 2.4 at $F_D = 1.0$. In the second, the bubbles retain their circular shape and are each largely

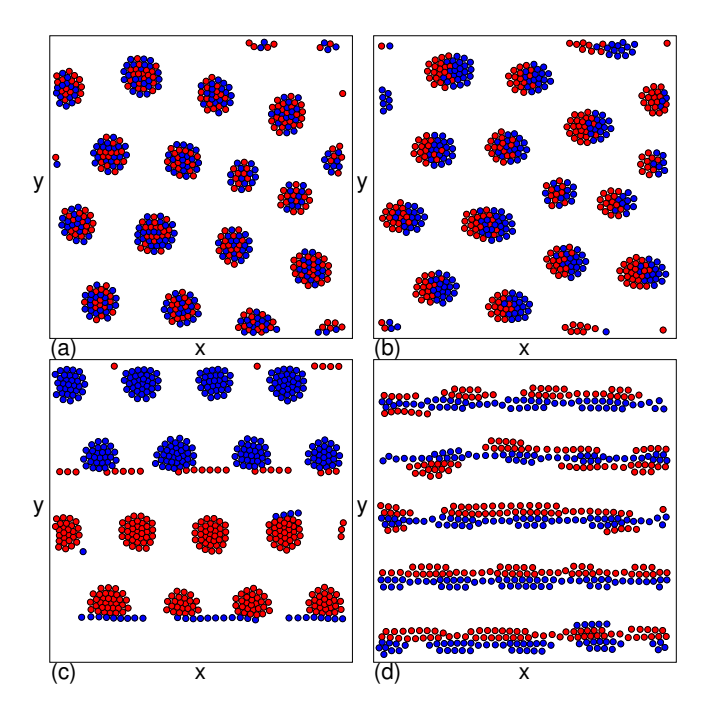


FIG. 12. Particle positions for the system in Fig. 11 with $\rho=0.441$. Red (blue) particles are driven in the negative (positive) x direction. (a) Spatially mixed bubbles at $F_D=0.03$ and B=2.35. (b) Polarized or segregated bubbles at $F_D=0.1$ and B=2.35. (c) The laned bubble state with a small number of stripes at $F_D=2.5$ and B=2.35. (d) The laned state at $F_D=1.5$ and a smaller B=2.25.

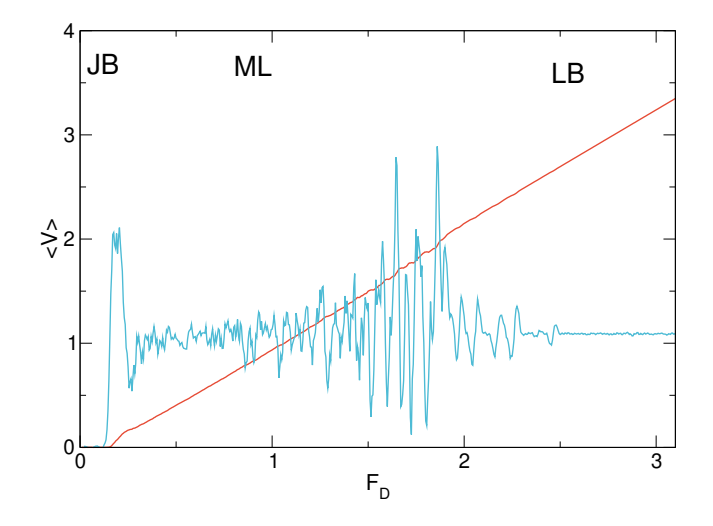


FIG. 13. $\langle V \rangle$ (red) and $d \langle V \rangle / dF_D$ (blue) vs F_D for the system from Figs. 11 and 12 with $\rho = 0.441$ at B = 2.35, showing the jammed bubble (JB), fluctuating moving liquid (ML), and laned bubble (LB) states.

composed of a single particle species with a few particles of the opposite species remaining trapped in each bubble, as shown in Fig. 14(b) for B=2.6 at $F_D=1.0$.

In Fig. 15, we show the jammed bubble phase from the system in Fig. 11 at B=2.8 and $F_D=0.0$, where a

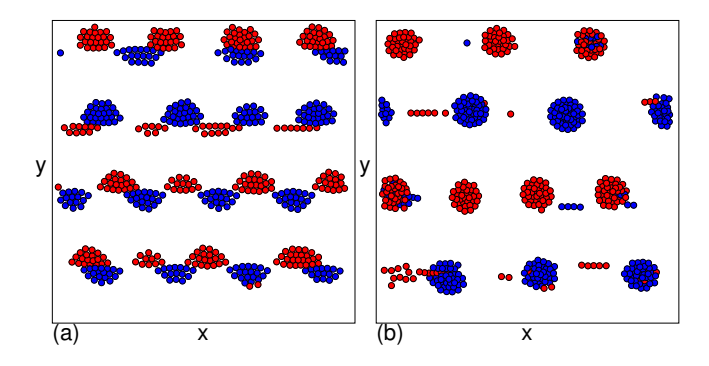


FIG. 14. Particle positions for the system from Fig. 11 with $\rho=0.441$ at $F_D=1.0$ in the laned bubble state. Red (blue) particles are driven in the negative (positive) x direction. (a) B=2.4. (b) B=2.6.

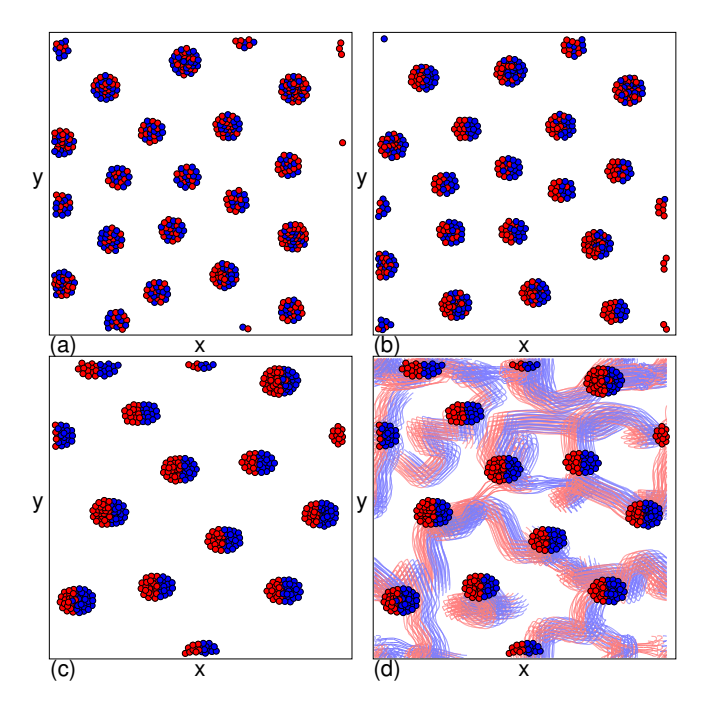


FIG. 15. Particle positions for the system from Fig. 11 with $\rho=0.441$ at B=2.8. Red (blue) particles are driven in the negative (positive) x direction. (a) A mixed bubble state at $F_D=0.0$. (b) At $F_D=0.25$, the particles in the bubbles start to rearrange into a polarized jammed bubble state. (c) The fully polarized bubble state at $F_D=0.45$, just below the unjamming transition. (d) At $F_D=0.5$ in the plastic bubble phase, the particles remain confined to the bubbles, but the bubbles move past one another. Lines illustrate the particle trajectories, with light red (light blue) lines indicating the motion of particles driven in the negative (positive) x direction.

bubble lattice appears that is composed of bubbles with spatially mixed particle species. As F_D increases, the bubbles undergo rearrangements and the particle species begin to segregate, as shown in Fig. 15(b) at $F_D = 0.25$, but the system remains jammed. The bubbles become increasingly segregated and elongated as the drive in-

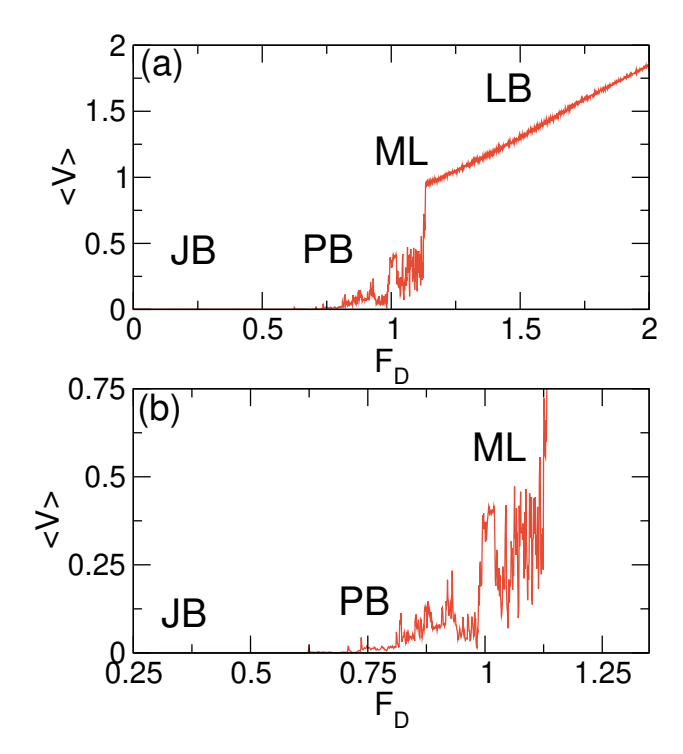


FIG. 16. (a) $\langle V \rangle$ vs F_D for the system in Fig. 15 at $\rho=0.411$ and B=2.8, with letters indicating the jammed bubble (JB), plastic bubble (PB), moving liquid (ML), and laned bubble (LB) phases. (b) A blowup of the lower drive region from panel (a) showing the plastic bubble depinning regime in more detail.

creases further, as illustrated in Fig. 15(c) at $F_D = 0.45$. Above the critical unjamming force F_c , the particles remain in the bubbles but the bubbles begin to move past one another, as shown in Fig. 15(d) at $F_D = 0.5$, where we highlight the particle locations and trajectories over time. When B > 2.6, as is the case in Fig. 15, the particles are so tightly bound to the bubbles that they are unable to escape from their original bubble. Since there are different numbers of particles of each species in each bubble, there is a force imbalance such that some bubbles experience a net negative x direction force while others have a net positive x direction force. This causes the bubbles to move past one another. The long range Coulomb repulsion between adjacent bubbles is also unbalanced because not all of the bubbles contain the same total number of particles, and this results in a distortion of what would otherwise be a roughly triangular lattice of bubbles. For higher drives, the system transitions into a disordered moving liquid state and then reorganizes into a laned bubble state, as shown in Fig. 14(b).

In Fig. 16(a), we plot the velocity-force curve $\langle V \rangle$ versus F_D for the system in Fig. 15 with $\rho=0.411$ and B=2.8 where there is a plastic bubble phase. Figure 16(b) shows a blowup of the lower drive regime where the plastic bubble motion occurs. Here, $\langle V \rangle$ remains low since the bubbles are only slowly moving past each other,

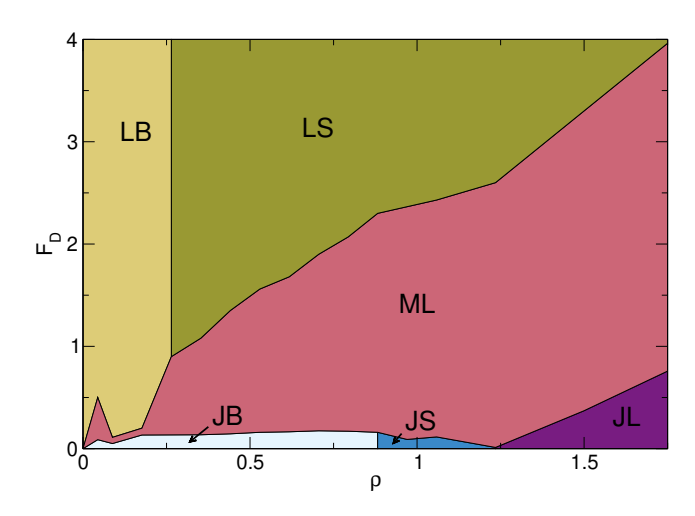


FIG. 17. Dynamic phase diagram as a function of F_D vs ρ for a system with B=2.3. JB: jammed bubble phase (pale blue), JS: jammed stripe phase (dark blue), JL: jammed labyrinth phase (dark purple), ML: disordered moving liquid phase (red), LB: laned bubble phase (yellow), and LS: laned stripe phase (olive green).

but there are occasional fluctuations in which sudden bursts of motion occur. At higher drives, the particles begin to escape from the bubbles, and the velocity increases as the system enters the moving liquid state.

VI. VARIED BUBBLE DENSITY

We next examine the evolution of the phases for varied density at B=2.3, where a jammed bubble state appears when $\rho = 0.441$. In Fig. 17, we show the dynamic phase diagram as a function of F_D versus ρ . At $F_D = 0$, there is a jammed bubble phase for $0 < \rho \le 0.9$, a jammed stripe phase for $0.9 < \rho \le 1.2$, and a jammed labyrinth for $\rho >$ 1.2. The critical unjamming force is non-monotonic and passes through a local minimum near the transition from a jammed stripe to a jammed labyrinth state. Above the unjamming transition, there is a disordered moving liquid phase that is followed at higher drives by a moving laned bubble state for $\rho < 0.25$ and by a laned stripe phase for $\rho > 0.25$. The moving liquid phase grows in extent with increasing ρ . We note that within the laned stripe phase, there is an extended region where the system has stripelike structure, but the particles within each stripe are strongly fluctuating. For values of ρ higher than what we consider in this work, it is likely that a uniformly jammed state would appear that would transition into a uniformly laned state at high drives. In Fig. 18(a), we illustrate the jammed labyrinth phase at $\rho = 1.235$ and $F_D = 0.0$. Figure 18(b) shows the disordered moving liquid phase at $F_D = 0.2$ near the unjamming point, while Fig. 18(c) shows the alignment in the moving liquid phase for intermediate drives of $F_D = 0.8$. The high drive laned stripe state appears in Fig. 18(d) at $F_D = 3.0$.

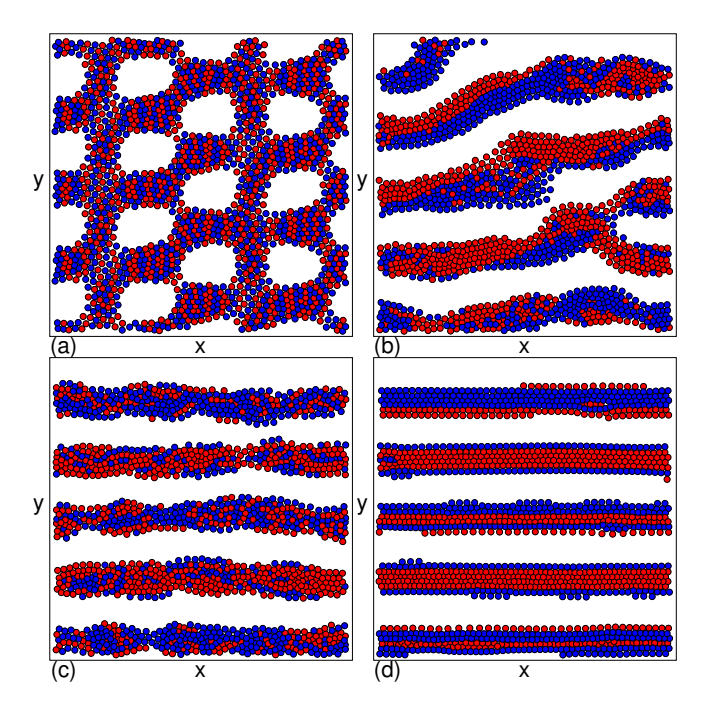


FIG. 18. Particle positions for the system from Fig. 17 with B=2.3 at $\rho=1.234$. Red (blue) particles are driven in the negative (positive) x direction. (a) Jammed labyrinth phase at $F_D=0.0$. (b) Disordered moving liquid phase at $F_D=0.2$. (c) Disordered moving liquid state at $F_D=0.8$, where the particles align with the driving direction. (d) Laned stripe state at $F_D=3.0$.

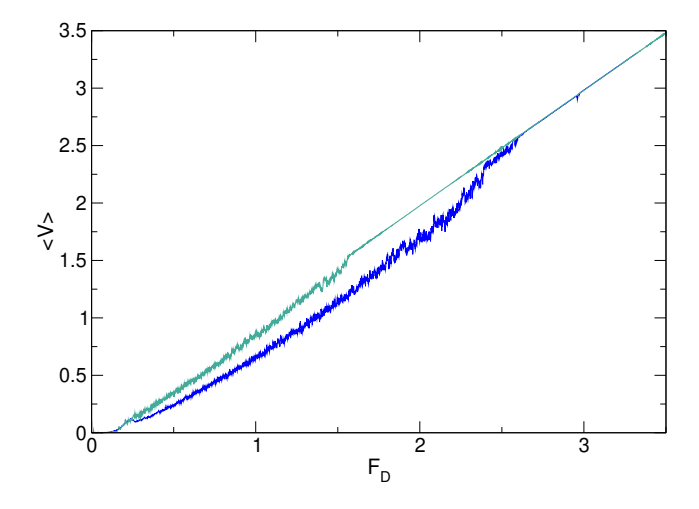


FIG. 19. $\langle V \rangle$ vs F_D for the system from Fig. 17 with B=2.3 at $\rho=0.47$ (green) and $\rho=1.29$ (blue).

In Fig. 19, we plot $\langle V \rangle$ versus F_D for the B=2.3 system from Fig. 17 at $\rho=0.47$ and $\rho=1.29$. For both densities, the onset of the ordered laned stripe phase is visible as a drop in the velocity fluctuations. The disordered moving liquid regime is smaller for $\rho=0.47$ compared to $\rho=1.29$, and the ordering into the laned stripe phase occurs at lower drives.

We find some interesting ordered jammed and laned

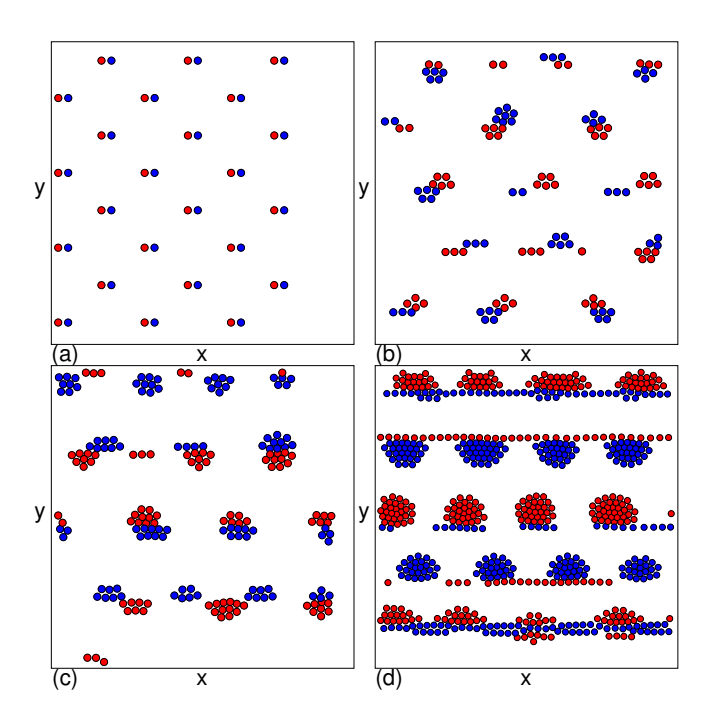


FIG. 20. Particle positions for the system from Fig. 17 with B=2.3. Red (blue) particles are driven in the negative (positive) x direction. (a) Jammed dimer phase at $\rho=0.044$ and $F_D=0.05$. (b) Laned bubble phase at $\rho=0.264$ and $F_D=1.5$, at the border with the laned stripe phase. (d) Laned stripe state at $\rho=0.529$ and $F_D=2.0$.

states at low densities in the B=2.3 system from Fig. 17. In Fig. 20(a), we show that the jammed phase at $\rho=0.044$ consists of polarized dimers. An example of the moving laned bubble state at $F_D=1.5$ appears in Fig. 20(b) for $\rho=0.88$, where the bubbles are quite fragmentary. For $\rho=0.264$ and $F_D=1.5$, at the border separating the laned bubble and laned stripe states, Fig. 20(c) shows that the bubbles have become more cohesive and are beginning to elongate. Figure 20(d) shows the laned stripe state at $\rho=0.529$ and $F_D=2.0$.

Another unusual ordered bubble state we observed appears in Fig. 21(a), where we show the particle configurations at $\rho=0.09$, B=2.4, and $F_D=0.15$. Figure 21(b) shows the corresponding particle trajectories. Each bubble captures four particles that are divided unevenly: there are three particles of one species, and one particle of the other species. The resulting force imbalance on each bubble produces motion, and the system has organized into alternating rows containing bubbles of equal composition. This is an example of a laned plastic bubble state.

In Fig. 22, we show a dynamic phase diagram as a function of F_D versus ρ at B=2.8. In this case, B is large enough to produce an extended window of plastic bubble phase. As ρ increases, the size of the bubbles increases, and the critical unjamming force F_c also increases. When $\rho > 0.6$, however, F_c begins to decrease with increasing

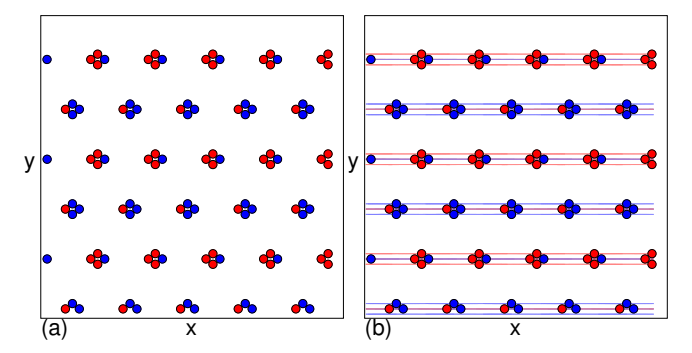


FIG. 21. Particle positions in the laned plastic bubble state at B=2.4, $\rho=0.09$, and $F_D=0.15$. Red (blue) particles are driven in the negative (positive) x direction. (b) The same system with lines indicating the particle trajectories, where light red (light blue) lines illustrate the motion of particles driven in the negative (positive) x direction. The bubbles each contain three particles of one species and one particle of the other species, and the resulting force imbalance leads to ordered flow.

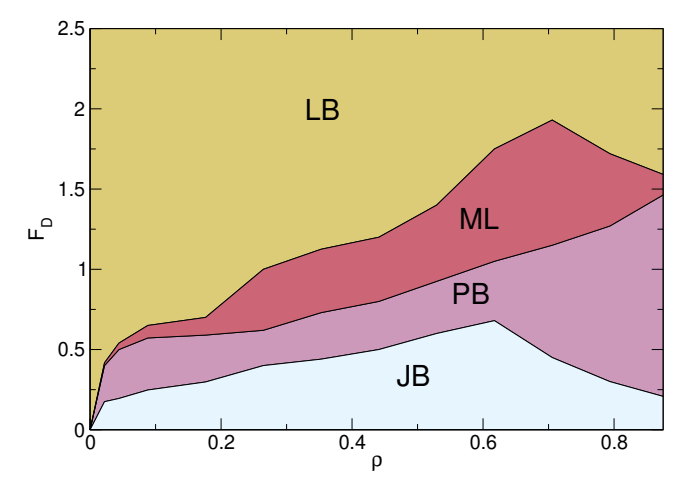


FIG. 22. Dynamic phase diagram as a function of F_D vs ρ at B=2.8, highlighting the extended plastic bubble phase. JB: jammed bubble phase (pale blue), PB: plastic bubble phase (purple), ML: disordered moving liquid phase (red), and LB: laned bubble phase (yellow).

 ρ , but since the onset of the moving liquid phase continues to shift to higher F_D with increasing ρ , the width of the plastic bubble phase increases as the density becomes higher.

We have also considered a system in which we fix B=2.0 and $\rho=0.441$ while varying $1/\kappa$. In Fig. 23, we plot the resulting dynamic phase diagram as a function of F_D versus $1/\kappa$. The uniform jammed state that appears for $0.7 < 1/\kappa < 0.975$ unjams into a moving liquid state and then transitions at higher drives to a uniform laned state. For $0.975 \le 1/\kappa < 1.1$, we find a jammed stripe state, and for $1/\kappa > 1.1$, there is a jammed bubble state. The critical unjamming threshold drops at the transition from the uniform jammed state to the jammed stripe state,

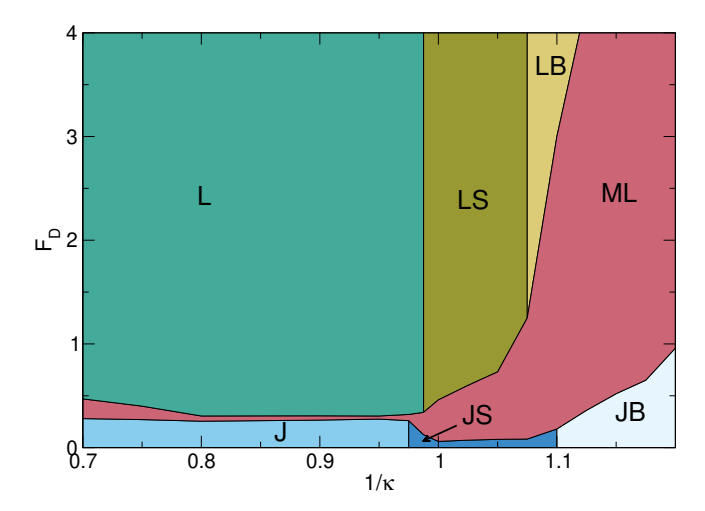


FIG. 23. Dynamic phase diagram as a function of F_D vs $1/\kappa$ for a system with B=2.0 and $\rho=0.441$. JB: jammed bubble phase (pale blue), JS: jammed stripe phase (dark blue), J: jammed uniform phase (medium blue), ML: disordered moving liquid phase (red), LB: laned bubble phase (yellow), LS: laned stripe phase (olive green), and L: uniform laned state (green). The critical unjamming force shows a dip in the stripe phase.

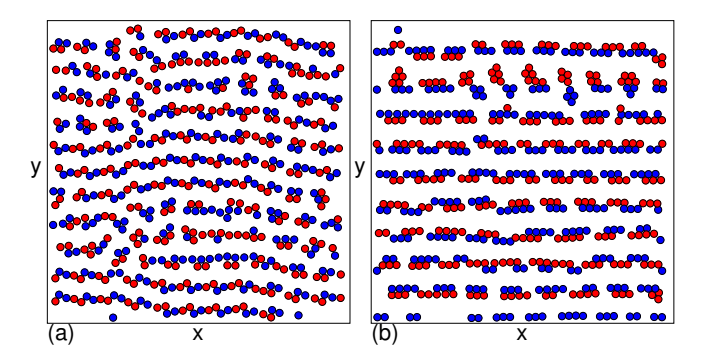


FIG. 24. Particle positions for a system with $\rho=0.441$, $1/\kappa=0.52$, and B=6.0. Red (blue) particles are driven in the negative (positive) x direction. (a) Jammed stripe state at $F_D=0.05$. (b) Moving laned stripe state at $F_D=1.0$.

and then begins to increase again in the bubble phase. The jammed stripe state unjams into a disordered moving liquid state and then organizes into a laned stripe state for lower $1/\kappa$ and into a laned bubble state for larger $1/\kappa$.

There are also a number of variations of the stripe and bubble states that can arise in our system for varied B and $1/\kappa$. An example of this is shown in Fig. 24(a) for B=6.0, $\rho=0.441$, and $1/\kappa=0.52$ at $F_D=0.05$, where a jammed stripe state appears that has some local dimer structuring. Figure 24(b) shows that at a higher drive of $F_D=1.0$, this system forms a laned stripe state that resembles the laned stripes found in the $\kappa=1.0$ system, but with lanes that are greatly reduced in width.

VII. DISCUSSION

We considered a specific type of SALR interaction; however, there are many other interactions that give similar patterns, and we expect that such interactions would produce effects similar to those described above. A possible difference is that the jamming state may occur at much lower density and could be much more strongly heterogeneous for two-step repulsive potentials with finite range. In certain cases, it may be easier in experiment to apply ac rather than dc driving. Since the patterns formed by our system have multiple length scales, ac driving could produce additional effects not found for single-scale strictly repulsive interaction potentials. For example, there could be one type of behavior at ac amplitudes where the particle motion is on roughly the same scale as the spacing of individual particles within a mesophase, but different behavior could appear at higher ac amplitudes when the motion reaches the same scale as the mesophase, such as the distance between stripes or bubbles. We focused on the case of 50:50 mixtures of driven particles, but if one species is more prevalent than the other, we expect that some of the phases we observe could be modified. We did not consider thermal fluctuations, but we expect that if the fluctuations are weak, the same phases would arise. At higher temperatures, it is likely that the laned stripe state would be the most susceptible to transitioning into a disordered fluctuating quasi-one-dimensional state. Beyond soft matter systems, our results could be relevant for certain types of pedestrian flows, where instead of individual particles driven in opposite directions, there are groups with some associations, leading to an effective short range attraction between people.

VIII. SUMMARY

We have examined the laning and dynamic phases for an assembly of particles with competing short-range attraction and long-range repulsion where half of the particles are driven in a direction opposite to the other half. In the absence of driving, this system forms crystal, stripe. and bubble states depending on the density and the ratio of attraction to repulsion. In previous work for oppositely driven particles with single-scale repulsive interactions, it was shown that a laning state forms at high drives and a disordered state appears at low drives. For the system with competing interactions, we find a much wider variety of states. At high densities or when the repulsive term dominates, as the drive increases the system passes through a uniform jammed state, a disordered moving liquid state, and a high-drive laned state. The transitions between these states produce signatures in the velocity-force curve, differential mobility, and density of topological defects. For intermediate ratios of attraction to repulsion, the system forms a jammed state that breaks up near the unjamming transition. At higher

drives, there is a fluid-like stripe state and then a laned stripe state where each stripe contains well-defined lanes of oppositely moving particles. For stronger attraction, the system forms a jammed bubble state. As the drive increases, the particles remain jammed but rearrange and segregate inside the bubbles to form a strongly polarized elongated bubble state just before unjamming. The system unjams into a fluctuating state or a plastic bubble state, depending on the ability of the particles to jump from bubble to bubble. A variety of laned bubble states can appear, including bubbles that move through each other or a more fully segregated state where each lane contains bubbles of a single particle species. The unjamming threshold force is strongly non-monotonic, passing through a minimum in the stripe regime and increasing in the bubble regime. We map out the evolution of the dynamic phases as a function of the ratio of attraction to repulsion, particle density, screening length, and drive.

ACKNOWLEDGMENTS

We gratefully acknowledge the support of the U.S. Department of Energy through the LANL/LDRD program for this work. This work was supported by the US Department of Energy through the Los Alamos National Laboratory. Los Alamos National Laboratory is operated by Triad National Security, LLC, for the National Nuclear Security Administration of the U.S. Department of Energy (Contract No. 892333218NCA000001).

- D. Helbing, I. J. Farkas, and T. Vicsek, Freezing by heating in a driven mesoscopic system, Phys. Rev. Lett. 84, 1240 (2000).
- [2] J. Dzubiella, G. P. Hoffmann, and H. Löwen, Lane formation in colloidal mixtures driven by an external field, Phys. Rev. E 65, 021402 (2002).
- [3] J. Chakrabarti, J. Dzubiella, and H. Löwen, Reentrance effect in the lane formation of driven colloids, Phys. Rev. E 70, 012401 (2004).
- [4] T. Glanz and H. Löwen, The nature of the laning transition in two dimensions, J. Phys: Condens. Matter 24, 464114 (2012).
- [5] M. Ikeda, H. Wada, and H. Hayakawa, Instabilities and turbulence-like dynamics in an oppositely driven binary particle mixture, EPL 99, 68005 (2012).
- [6] K. Klymko, P. L. Geissler, and S. Whitelam, Microscopic origin and macroscopic implications of lane formation in mixtures of oppositely driven particles, Phys. Rev. E 94, 022608 (2016).
- [7] A. Poncet, O. Bénichou, V. Démery, and G. Oshanin, Universal long ranged correlations in driven binary mixtures, Phys. Rev. Lett. 118, 118002 (2017).
- [8] M. Isele, K. Hofmann, A. Erbe, P. Leiderer, and P. Nielaba, Lane formation of colloidal particles driven in parallel by gravity, Phys. Rev. E 108, 034607 (2023).
- [9] H. Yu and R. L. Jack, Competition between lanes and transient jammed clusters in driven binary mixtures, Phys. Rev. E 109, 024123 (2024).
- [10] M. E. Leunissen, C. G. Christova, A. P. Hynninen, C. P. Royall, A. I. Campbell, A. Imhof, M. Dijkstra, R. van Roij, and A. van Blaaderen, Ionic colloidal crystals of oppositely charged particles, Nature (London) 437, 235 (2005).
- [11] M. Rex and H. Löwen, Lane formation in oppositely charged colloids driven by an electric field: Chaining and two-dimensional crystallization, Phys. Rev. E 75, 051402 (2007).
- [12] H. Löwen, Particle-resolved instabilities in colloidal dispersions, Soft Matter 6, 3133 (2010).
- [13] T. Vissers, A. van Blaaderen, and A. Imhof, Band formation in mixtures of oppositely charged colloids driven by an ac electric field, Phys. Rev. Lett. 106, 228303 (2011).

- [14] T. Geigenfeind, D. de las Heras, and M. Schmidt, Superadiabatic demixing in nonequilibrium colloids, Commun. Phys. 3, 23 (2020).
- [15] K. R. Sütterlin, A. Wysocki, A. V. Ivlev, C. Räth, H. M. Thomas, M. Rubin-Zuzic, W. J. Goedheer, V. E. Fortov, A. M. Lipaev, V. I. Molotkov, O. F. Petrov, G. E. Morfill, and H. Löwen, Dynamics of lane formation in driven binary complex plasmas, Phys. Rev. Lett. 102, 085003 (2009).
- [16] N. P. Vizarim, J. C. B. Souza, C. J. O. Reichhardt, C. Reichhardt, P. A. Venegas, and F. Béron, Skyrmionskyrmionium phase separation and laning transitions via spin-orbit torque currents, Phys. Rev. B 111, 214438 (2025).
- [17] C. Reichhardt and C. J. O. Reichhardt, Velocity force curves, laning, and jamming for oppositely driven disk systems, Soft Matter 14, 490 (2018).
- [18] C. Feliciani and K. Nishinari, Empirical analysis of the lane formation process in bidirectional pedestrian flow, Phys. Rev. E 94, 032304 (2016).
- [19] K. A. Bacik, B. S. Bacik, and T. Rogers, Lane nucleation in complex active flows, Science 379, 923 (2023).
- [20] N. Bain and D. Bartolo, Critical mingling and universal correlations in model binary active liquids, Nature Commun. 8, 15969 (2017).
- [21] C. Reichhardt, J. Thibault, S. Papanikolaou, and C. J. O. Reichhardt, Laning and clustering transitions in driven binary active matter systems, Phys. Rev. E 98, 022603 (2018).
- [22] B. Khelfa, R. Korbmacher, A. Schadschneider, and A. Tordeux, Heterogeneity-induced lane and band formation in self-driven particle systems, Sci. Rep. 12, 4768 (2022).
- [23] T. Glanz, R. Wittkowski, and H. Löwen, Symmetry breaking in clogging for oppositely driven particles, Phys. Rev. E 94, 052606 (2016).
- [24] A. Wysocki and H. Löwen, Oscillatory driven colloidal binary mixtures: Axial segregation versus laning, Phys. Rev. E 79, 041408 (2009).
- [25] B. Li, Y.-L. Wang, G. Shi, Y. Gao, X. Shi, C. E. Woodward, and J. Forsman, Phase transitions of oppositely charged colloidal particles driven by alternating current

- electric field, ACS Nano 15, 2363 (2021).
- [26] C. J. O. Reichhardt and C. Reichhardt, Disordering, clustering, and laning transitions in particle systems with dispersion in the Magnus term, Phys. Rev. E 99, 012606 (2019).
- [27] C. W. Wächtler, F. Kogler, and S. H. L. Klapp, Lane formation in a driven attractive fluid, Phys. Rev. E 94, 052603 (2016).
- [28] F. Kogler and S. H. L. Klapp, Lane formation in a system of dipolar microswimmers, EPL 110, 10004 (2015).
- [29] M. Seul and D. Andelman, Domain shapes and patterns - the phenomenology of modulated phases, Science 267, 476 (1995).
- [30] A. D. Stoycheva and S. J. Singer, Stripe melting in a twodimensional system with competing interactions, Phys. Rev. Lett. 84, 4657 (2000).
- [31] C. Reichhardt, C. J. Olson, I. Martin, and A. R. Bishop, Depinning and dynamics of systems with competing interactions in quenched disorder, Europhys. Lett. 61, 221 (2003).
- [32] C. J. O. Reichhardt, C. Reichhardt, I. Martin, and A. R. Bishop, Dynamics and melting of stripes, crystals, and bubbles with quenched disorder, Physica D 193, 303 (2004).
- [33] S. Mossa, F. Sciortino, P. Tartaglia, and E. Zaccarelli, Ground-state clusters for short-range attractive and longrange repulsive potentials, Langmuir **20**, 10756 (2004).
- [34] F. Sciortino, S. Mossa, E. Zaccarelli, and P. Tartaglia, Equilibrium cluster phases and low-density arrested disordered states: The role of short-range attraction and long-range repulsion, Phys. Rev. Lett. 93, 055701 (2004).
- [35] K. Nelissen, B. Partoens, and F. M. Peeters, Bubble, stripe, and ring phases in a two-dimensional cluster with competing interactions, Phys. Rev. E 71, 066204 (2005).
- [36] Y. H. Liu, L. Y. Chew, and M. Y. Yu, Self-assembly of complex structures in a two-dimensional system with competing interaction forces, Phys. Rev. E 78, 066405 (2008).
- [37] C. J. Olson Reichhardt, C. Reichhardt, and A. R. Bishop, Structural transitions, melting, and intermediate phases for stripe- and clump-forming systems, Phys. Rev. E 82, 041502 (2010).
- [38] D. McDermott, C. J. O. Reichhardt, and C. Reichhardt, Stripe systems with competing interactions on quasi-one dimensional periodic substrates, Soft Matter 10, 6332 (2014).
- [39] Y. Liu and Y. Xi, Colloidal systems with a short-range attraction and long-range repulsion: phase diagrams, structures, and dynamics, Curr. Opin. Colloid Interf. Sci. 19, 123 (2019).
- [40] A. Hooshanginejad, J.-W. Barotta, V. Spradlin, G. Pucci, R. Hunt, and D. M. Harris, Interactions and pattern formation in a macroscopic magnetocapillary salr system of mermaid cereal, Nature Commun. 15, 5466 (2024).
- [41] E. A. Jagla, Phase behavior of a system of particles with core collapse, Phys. Rev. E 58, 1478 (1998).
- [42] G. Malescio and G. Pellicane, Stripe phases from isotropic repulsive interactions, Nature Mater. 2, 97 (2003).
- [43] M. A. Glaser, G. M. Grason, R. D. Kamien, A. Kosmrlj, C. D. Santangelo, and P. Ziherl, Soft spheres make more mesophases, EPL 78, 46004 (2007).

- [44] L. Q. Costa Campos, S. W. S. Apolinario, and H. Löwen, Structural ordering of trapped colloids with competing interactions, Phys. Rev. E 88, 042313 (2013).
- [45] A. Al Harraq, A. A. Hymel, E. Lin, T. M. Truskett, and B. Bharti, Dual nature of magnetic nanoparticle dispersions enables control over short-range attraction and long-range repulsion interactions, Commun. Chem. 5, 72 (2022).
- [46] M. M. Fogler, A. A. Koulakov, and B. I. Shklovskii, Ground state of a two-dimensional electron liquid in a weak magnetic field, Phys. Rev. B 54, 1853 (1996).
- [47] R. Moessner and J. T. Chalker, Exact results for interacting electrons in high Landau levels, Phys. Rev. B 54, 5006 (1996).
- [48] K. B. Cooper, M. P. Lilly, J. P. Eisenstein, L. N. Pfeiffer, and K. W. West, Insulating phases of two-dimensional electrons in high Landau levels: Observation of sharp thresholds to conduction, Phys. Rev. B 60, R11285 (1999).
- [49] E. Fradkin and S. A. Kivelson, Liquid-crystal phases of quantum Hall systems, Phys. Rev. B 59, 8065 (1999).
- [50] J. Göres, G. Gamez, J. H. Smet, L. Pfeiffer, K. West, A. Yacoby, V. Umansky, and K. von Klitzing, Currentinduced anisotropy and reordering of the electron liquidcrystal phases in a two-dimensional electron system, Phys. Rev. Lett. 99, 246402 (2007).
- [51] B. Friess, V. Umansky, K. von Klitzing, and J. H. Smet, Current flow in the bubble and stripe phases, Phys. Rev. Lett. 120, 137603 (2018).
- [52] X. B. Xu, T. Tang, Z. H. Wang, X. N. Xu, G. Y. Fang, and M. Gu, Nonequilibrium pattern formation in circularly confined two-dimensional systems with competing interactions, Phys. Rev. E 103, 012604 (2021).
- [53] L. Komendová, Y. Chen, A. A. Shanenko, M. V. Milošević, and F. M. Peeters, Two-band superconductors: Hidden criticality deep in the superconducting state, Phys. Rev. Lett. 108, 207002 (2012).
- [54] C. N. Varney, K. A. H. Sellin, Q.-Z. Wang, H. Fangohr, and E. Babaev, Hierarchical structure foramtion in layered superconducting systems with multi-scale intervortex interactions, J. Phys.: Condens. Matter 25, 415702 (2013).
- [55] K. A. H. Sellin and E. Babaev, Stripe, gossamer, and glassy phases in systems with strong nonpairwise interactions, Phys. Rev. E 88, 042305 (2013).
- [56] X. S. Brems, S. Mühlbauer, W. Y. Córdoba-Camacho, A. A. Shanenko, A. Vagov, J. A. Aguiar, and R. Cubitt, Current-induced self-organisation of mixed superconducting states, Supercond. Sci. Technol. 35, 035003 (2022).
- [57] D. McDermott, C. J. O. Reichhardt, and C. Reichhardt, Structural transitions and hysteresis in clump- and stripe-forming systems under dynamic compression, Soft Matter 12, 9549 (2016).
- [58] C. Reichhardt and C. J. O. Reichhardt, Peak effect and dynamics of stripe- and pattern-forming systems on a periodic one-dimensional substrate, Phys. Rev. E 109, 054606 (2024).
- [59] C. Reichhardt and C. J. O. Reichhardt, Stripe and bubble ratchets on asymmetric substrates, Phys. Rev. Res. 6, 043290 (2024).
- [60] C. Reichhardt and C. J. O. Reichhardt, Aspects of jamming in two-dimensional athermal frictionless systems, Soft Matter 10, 2932 (2014).

- [61] K. A. Dahmen, Y. Ben-Zion, and J. T. Uhl, A simple analytic theory for the statistics of avalanches in sheared granular materials, Nature Phys. 7, 554 (2011).
- [62] C. Reichhardt and C. J. O. Reichhardt, Depinning and nonequilibrium dynamic phases of particle assemblies driven over random and ordered substrates: a review,
- Rep. Prog. Phys. **80**, 026501 (2017).
- [63] C. J. O. Reichhardt, D. McDermott, and C. Reichhardt, Using principal component analysis to distinguish different dynamic phases in superconducting vortex matter, Phys. Rev. B 111, 104508 (2025).